JBC Papers in Press. Published on July 16, 2010 as Manuscript M110.118844
The latest version is at http://www.jbc.org/cgi/doi/10.1074/jbc.M110.118844

Unique Structural Characteristics of the Rabbit Prion Protein

Yi Wen[1,†], Jun Li[1,†,§], Wenming Yao[1], Minqian Xiong[1], Jing Hong[1], Yu Peng[1], Gengfu Xiao[2], and Donghai Lin[1,3,*]

From [1]NMR Laboratory, Shanghai Institute of Materia Medica, Chinese Academy of Sciences, Shanghai 201203, and [2]State Key Laboratory of Virology, College of Life Science, Wuhan University, Wuhan 430072, and [3]Key Laboratory of Chemical Biology of Fujian Province, College of Chemistry and Chemical Engineering, Xiamen University, Xiamen 361005, China.

Running head: Unique rabbit prion protein

[*]Address correspondence to: Donghai Lin, Shanghai Institute of Materia Medica, Chinese Academy of Sciences, 555 Zu Chongzhi Road, Shanghai 201203, China. Tel/Fax number: +86-21-50806036; E-mail address: dhlin@mail.shcnc.ac.cn

Rabbits are one of the few mammalian species that appear to be resistant to transmissible spongiform encephalopathies (TSEs) due to the structural characteristics of the rabbit prion protein ($RaPrP^C$) itself. Here we determined the solution structures of the recombinant protein $RaPrP^C$-(91-228) and its S173N variant, and detected the backbone dynamics of their structured C-terminal domains-(121-228). In contrast to many other mammalian PrP^Cs, loop 165-172 that connects β-sheet-2 and α-helix-2 is well-defined in $RaPrP^C$. For the first time, order parameters S^2 are obtained for residues in this loop region, indicating that loop 165-172 of $RaPrP^C$ is highly ordered. Compared with the wild-type $RaPrP^C$, less hydrogen bonds form in the S173N variant. The NMR dynamics analysis reveals a distinct increase in the structural flexibility of loop 165-172 and helix-3 after the S173N substitution, implying that the S173N substitution disturbs the long-range interaction of loop 165-172 with helix-3, which further leads to a marked decrease in the global conformational stability. Significantly, $RaPrP^C$ possesses a unique charge distribution, carrying a continuous area of positive charges on the surface, which is distinguished from other PrP^Cs. The S173N substitution causes visible changes of the charge distribution around the recognition sites for the hypothetical protein X. Our results suggest that the ordered loop 165-172 and its interaction with helix-3, together with the unique distribution of surface electrostatic potential, significantly contribute to the unique structural characteristics of $RaPrP^C$.

Transmissible spongiform encephalopathies (TSEs) or prion diseases, which include scrapie in sheep, bovine spongiform encephalopathy (BSE) in cattle and Creutzfeldt-Jakob disease (CJD) in humans, are an unusual group of fatal neurodegenerative disorders that can be sporadic, inherited or acquired. The infectious agent has been uniquely identified as the scrapie prion protein (PrP^{Sc}), a pathogenic isoform of the host-encoded cellular prion protein (PrP^C) (1,2). PrP^C and PrP^{Sc} seem to possess the same covalent structure but differ substantially in conformation. PrP^C is monomeric and soluble, sensitive to proteolysis with proteinase K, while PrP^{Sc} is highly insoluble and readily forming proteinase-resistant aggregates. Both circular dichroism (CD) spectra and Fourier transform infrared (FTIR) spectra show that PrP^C is predominantly α-helical, whereas PrP^{Sc} possesses a considerable amount of β-sheet content (3-5).

PrP^C is mostly expressed in the central nervous system. It is a highly conserved cell surface glycoprotein, attached to the outer leaflet of the cell membrane via a glycosylphosphatidylinositol (GPI) anchor at its C-terminus. Although the physiological function of PrP^C remains unknown, its high affinity for copper (Ⅱ) indicates that it may act as a copper transport protein or a superoxide dismutase (6,7). Previous studies have indicated that PrP^C may be involved in pathways related to cell adhesion, synaptic integrity and cell signaling (8,9).

The conformational conversion of the prion protein, from PrP^C to PrP^{Sc}, has a crucial role in the pathogenesis of TSEs. Thus, knowledge of the three-dimensional structure of the prion protein is of great importance to understand the conformational conversion. Solution structures of

non-glycosolated PrP^Cs across a number of mammalian species, including mice, Syrian hamsters, humans, cattle, sheep, tammar wallabies, horses, etc., have been determined using NMR spectroscopy (10-16). Mature PrP^C consists of a single polypeptide chain of approximately 210 amino acids (residues 23-231). The N-terminus (residues 23-120) is flexible and disordered, with a highly conserved octa-repeating sequence PHGGGWGQ between residues 60 and 91. The C-terminus (residues 121-231) is a globular structured domain encompassing three α-helices and two short anti-parallel β-strands, with a disulfide bond bridging helices 2 and 3. Loop 165-172 and helix-3, so called conformational markers, are located on the surface of the structured C-terminal domain and reflect the differences among species (17).

Rabbits are one of the few mammalian species that appear to be resistant to TSE agents. So far no signs of TSE diseases have been observed in rabbits after inoculating them with the CJD, kuru or scrapie agents isolated from either mice or sheep (18). Both rabbit PrP^C ($RaPrP^C$) and chimeric rabbit-mouse PrP^C constructs are not converted to the proteinase-resistant form in scrapie-infected mouse neuroblastoma cells (Sc^+-MNB cells) which accumulate mouse PrP^{Sc} ($mPrP^{Sc}$) (19). These experiments suggest that the inability of the conformational conversion for $RaPrP^C$ and the resistance to the TSE infection for rabbits is most likely due to the structural characteristics of the $RaPrP^C$ protein itself. Thus, interpretation of the three-dimensional structure of $RaPrP^C$ would reveal the particular properties of $RaPrP^C$ distinguished from other PrP^Cs. In addition, sequence alignment shows that there are 22 different amino acid residues between $RaPrP^C$ and mouse PrP^C ($mPrP^C$). The $mPrP^C$ variants with multiple amino acid residues substituted by the corresponding residues in $RaPrP^C$ (N99G, L108M, N173S or V214I) are inhibited to convert to the abnormal form (19). These experimental observations imply that the specific amino acid residues at pivotal spots may somehow determine the structural characteristics of PrP^C. Therefore, a detailed understanding of tertiary structural differences between $RaPrP^C$ and $mPrP^C$, caused by the specific amino acid residues, could provide an essential insight into the molecular mechanism by which TSEs develop.

In this present work, we utilized multi-dimensional heteronuclear NMR techniques to determine the solution structures of the recombinant protein $RaPrP^C$-(91-228) and its S173N variant. Moreover, we used CD spectroscopy to assess their conformational stability upon urea-induced denaturation. In addition, we performed ^{15}N relaxation measurements to detect the backbone dynamics of their globular structured C-terminal domains-(121-228). Our results reveal the unique structural characteristics of $RaPrP^C$ and offer invaluable hints to understand the molecular mechanism of the conformational conversion for prion proteins.

Experimental procedures

Plasmid construction, protein expression and purification- The amplified gene fragment coding for $RaPrP^C$-(91-228) was inserted into the vector pET30a via *Nde* I and *Xho* I restriction sites. A single point mutant on this plasmid containing a serine 173 to asparagine substitution (S173N) was constructed via the site-directed mutagenesis PCR. Two other truncations，$RaPrP^C$-(121-228) and its S173N variant, were constructed using the vector pGBTNH via *BamH* I and *Xho* I restriction sites. The expression of recombinant proteins was carried out in the *E. coli* BL21(DE3) strain at 37 ℃. Unlabeled proteins were prepared in LB medium. Uniformly $^{15}N/^{13}C$-labeled and ^{15}N-labeled proteins were prepared by culturing cells in M9-minimal medium with ^{15}N-labeled ammonium chloride in the presence or absence of ^{13}C-labeled glucose, respectively. The on-column purification and refolding of recombinant proteins was performed as described previously (20), with the only modification by adding thrombin protease to remove the GB1 tag contained in the truncated proteins. Protein samples were desalted into Buffer F (20 mM NaOAc, 0.02% NaN_3, pH 4.5) and concentrated to 0.25 ml using Ultrafree-15 Centrifugal Filter Biomax Devices (Millipore). The protein purity was checked by polyacrylamide gel electrophoresis under denaturing condition and the protein concentration was measured by the BCA assay (Sigma). NMR samples at a concentration of 1 mM with 10% D_2O were used for structure determination and dynamics analysis.

NMR spectroscopy-All NMR measurements were carried out at 25 ℃ on a Varian Unity Inova 600

spectrometer equipped with three RF channels and a triple-resonance pulsed-field gradient probe. The spectra were processed with the program NMRPipe (21) and analyzed by the software Sparky (T. D. Goddard and D. G. Kneller, University of California, San Francisco). The three-dimensional heteronuclear NMR spectra, including HNCA, HN(CO)CA, HNCACB, CBCA(CO)NH, HBHA(CO)NH, HNCO and HN(CA)CO, were collected to obtain the sequence-specific backbone resonance assignments. The three-dimensional spectra H(CC)(CO)NH-TOCSY, (H)CC(CO)NH-TOCSY, HCCH-TOCSY, CCH-TOCSY and ^{15}N-edited TOCSY-HSQC were recorded for the side chain resonance assignments. Nearly complete backbone and side chain resonance assignments for RaPrP^{C}-(91-228) (22) and the S173N variant have been obtained. The three-dimensional ^{15}N- and ^{13}C-edited NOESY-HSQC experiments with a 100-ms mixing time were performed to confirm the resonance assignments and generate ^{1}H-^{1}H distance restraints for structure calculation. The hydrogen-deuterium (H-D) exchange experiments were conducted to obtain hydrogen bond restraints.

Structure determination- The three-dimensional structures of RaPrP^{C}-(91-228) and the S173N variant were calculated using NOE-derived distance restraints, in combination with dihedral angle restraints and hydrogen bond restraints by the ARIA/CNS software (23,24). A family of 200 structures was calculated according to the simulated annealing protocol. Fifteen structures of the lowest energy were selected, which exhibit no NOE violation greater than 0.3 Å and no dihedral angle violation greater than 5°. The final 15 structures were assessed by the PROCHECK program (25). The structural statistics are presented in Table 1. The ribbon and surface graphs were displayed using the software MolMol (26) or PyMol (kindly provided by Prof. DeLano WL). The atomic coordinates of RaPrP^{C}-(91-228) and the S173N variant have been deposited into the Protein Data Bank (PDB codes: 2FJ3 and 2JOH). The chemical shift data are available at the Biological Magnetic Resonance Data Bank (accession numbers: 7142 and 16328).

^{15}N relaxation measurements- All ^{15}N relaxation data were acquired at 25 ℃ on a Varian Unity Inova 600 spectrometer. The standard pulse sequences with minimal water suppression (27) were used to record the spectra of relaxation times T_1, T_2, and $\{^{1}H\}$-^{15}N heteronulear NOE. In the direct (^{1}H) dimension, the carrier frequency was set on the water resonance with a spectral width of 10,000 Hz. In the indirect (^{15}N) dimension, the spectral width was 1420 Hz. A recycle delay of 2 s was used. T_1 was measured using a series of spectra recorded with 10 relaxation delays：10.83, 54.17, 108.34, 216.68, 325.02, 541.70, 866.72, 1191.74, 1570.93 and 1950.12 ms. T_2 was determined with 10 relaxation delays：15.62, 31.23, 46.85, 62.46, 78.08, 93.70, 109.31, 124.93, 140.54 and 156.16 ms. The relaxation constants and the experimental errors were extracted by a single exponential curve fitting of the peak heights using the software Sparky. The steady-state $\{^{1}H\}$-^{15}N NOE enhancements were calculated as the ratio of peak heights in spectra recorded with or without proton saturation. The saturated spectra were acquired with a 2-sec relaxation delay followed by a 3-sec period of proton saturation. The spectra recorded in the absence of proton saturation employed a relaxation delay of 5 s. The standard errors were determined from two data sets.

Reduced spectral density mapping- The spectral density mapping approach can be used to describe the internal motions of N-H bonds without any assumptions about a specific molecular model. The heteronuclear relaxation parameters can be obtained from a weighted sum of the spectral density function $J(\omega)$ at five specific frequencies: 0, ω_N, ω_H, ω_H-ω_N, ω_H+ω_N. At high frequencies, however, the values of $J(0.87\omega_H)$, $J(\omega_H+\omega_N)$ and $J(\omega_H-\omega_N)$ can be assumed to be approximately equal in the case of ^{15}N relaxation (28-30). Thus, it is possible to map the spectral density function only using relaxation rates R_1, R_2 and heteronuclear NOEs. The reduced spectral density values can be expressed as follows:

$$\sigma=R_1(NOE-1)\gamma_N/\gamma_H \quad (1)$$

$$J(\omega_N)=(4R_1-5\sigma)/(3d^2+4c^2) \quad (2)$$

$$J(0)=(6R_2-3R_1-2.72\sigma)/(3d^2+4c^2) \quad (3)$$

$$J(0.87\omega_H)=4\sigma/5d^2 \quad (4)$$

where $d=\mu_0 h\gamma_N/\gamma_H\langle r_{NH}^{-3}\rangle/(8\pi^2)$, $c=\omega_N\triangle\sigma/3^{1/2}$, μ_0 is the permeability of the free space, h is the Planck's constant, γ_H and γ_N are the gyromagnetic ratios of ^{1}H and ^{15}N, respectively, r_{NH} is the N-H bond length, ω_H and ω_N are the Lamor frequencies of ^{1}H and ^{15}N, respectively, and $\triangle\sigma$ is the

chemical shift anisotropy for ^{15}N with $\triangle\sigma=\sigma_{//}-\sigma_{\perp}$=-160 ppm. We used the notebook provided by Spyracopoulos (31) to execute the calculation.

Modelfree analysis- The modelfree formalism is often used to describe internal motions of a protein. The spectral density functions are modeled differently depending on whether the rotational diffusion tensor is either isotropic or anisotropic. In the formalism of Lipari and Szabo (32,33), the spectral density function is given by

$$J(\omega)=\frac{2}{5}\left[\frac{S^2\tau_m}{1+(\omega\tau_m)^2}+\frac{(1-S^2)\tau}{1+(\omega\tau)^2}\right] \quad (5)$$

where $\tau^{-1} = \tau_m^{-1} + \tau_e^{-1}$, S^2 is the generalized order parameter that specifies the degree of spatial restriction of the N-H bond, τ_m is the correlation time for overall tumbling and τ_e is the correlation time for internal motion. Clore et al expanded this formalism to account for internal motion on two distinct time scales, which differ by at least one order of magnitude (34). An exchange term, R_{ex}, is also incorporated to account for slower conformational exchange processes which affect transverse relaxation times. The rotational diffusion tensors of $RaPrP^C$-(121-228) and the S173N variant were evaluated for a selected subset of spins with trimmed R_2/R_1 ratios (35) as well as NOE values larger than 0.6. We used the program Fastmodelfree (36) to perform the model selection and modelfree analysis.

Circular Dichroism- All CD spectra were recorded on a Jasco J-810 spectropolarimeter at 25 ℃. The reported spectra were an average of three consecutive scans and corrected for blank.

Far-UV CD spectra were collected in the wavelength range of 200-250 nm using a 0.1-cm pathlength quartz cuvette. For denaturation experiments, a high concentration stock of folded protein was diluted into Buffer F with or without urea, reaching to a final protein concentration of 0.2 $mg\cdot ml^{-1}$ and to a desired urea concentration. For renaturation, the high concentration urea in the stock of unfolded protein was diluted by added denaturant-free protein in Buffer F. The urea-induced unfolding transitions for secondary structure were analyzed by the mean residue ellipticity (θ) at 222 nm, assuming a two-state mechanism and a dependence of θ on denaturant concentration (37,38):

$$[\theta]=\frac{\left([\theta]_N^0+m_N[urea]\right)+\left([\theta]_U^0+m_U[urea]\right)\times\exp\left(-\left(\Delta G_{N\to U}^{H_2O}+m[urea]\right)/(RT)\right)}{1+\exp\left(-\left(\Delta G_{N\to U}^{H_2O}+m[urea]\right)/(RT)\right)} \quad (6)$$

where $[\theta]_N^0$ and $[\theta]_U^0$ are the ellipticity without denaturant at native or unfolded state, respectively, $\Delta G_{N\to U}^{H_2O}$ is an estimate of the free energy of unfolding extrapolated to zero concentration of denaturant, m_N and m_U are coefficients of the dependence of ellipticity on denaturant concentration at native or unfolded state, m is a measure of the dependence of $\Delta G_{N\to U}$ on denaturant concentration, R is the gas constant, and T is the absolute temperature.

Near-UV CD spectra were collected in the region of 260-350 nm using a 1-cm pathlength quartz cuvette. Stock solutions contained 1 $mg\cdot ml^{-1}$ protein with or without urea. Fresh mixtures of the stocks at the desired urea concentration were measured. The mean residue ellipticity at 268 nm was used for analysis.

Results

Solution structures- The three-dimensional structure of $RaPrP^C$-(91-228) comprises two short antiparallel β-strands (S1: residues 128-130, S2: 160-162) and three α-helices (H1: 144-153, H2: 173-186, H3: 199-227) (Fig. 1, A and B), similar to those of other mammalian prion proteins. Helices 2 and 3 are further stabilized by the disulfide bond between residues C178 and C213. The region 91-126 is highly disordered owing to lack of NOEs. Loop 165-172 and helix-3, designated as conformational markers (17), form a solvent-accessible contiguous epitope at the C-terminus of the prion protein. This area has been suggested to be the recognition sites for a hypothetical chaperone, protein X, which would moderate the conversion of PrP^C into the pathogenic PrP^{Sc} (39,40). Noticeably, loop 165-172 can be completely assigned in $RaPrP^C$ (Supplemental Fig. S1) by long-range NOEs from the residues at the end of helix-3.

$mPrP^C$ with the N173S substitution was not able to convert to the abnormal form (19). Thus, it is expected that the S173N substitution would cause structural change more or less for $RaPrP^C$. To evaluate the structural change we determined the solution structure of the S173N variant of

RaPrP^C-(91-228) (Fig. 1, C and D). Both three-dimensional structures are identical overall but with some local differences. The orientation of helix1 in the variant is divergent to that of the wild-type, with a deviation angle of around 24°. The end of helix-3 displays an irregular bend for either the wild-type or the variant, however, the bend is a bit sharper for the latter. Residues 191-193 may form a 3_{10} helix in the variant.

Surface charge distributions- It has been suggested that the distribution of electrostatic potential on the surface of the prion protein is related to the transmission barrier of TSEs (13,14,41,42). We compared the surface charge distributions among RaPrP^C and other mammalian PrP^{C}s including human PrP^C (hPrP^C), mPrP^C and bovine PrP^C (bPrP^C) (Fig. 2). Three-dimensional structures of these PrP^{C}s were determined in sodium acetate buffer at pH 4.5 (10,12,13). Amazingly, the distribution of electrostatic potential for RaPrP^C, with a large area of continuous positive charge on the surface (Fig. 2A), is significantly distinguished from those for other PrP^{C}s (Fig. 2). The area of continuous positive charge of RaPrP^C roughly covers residues 125-135, 150-160 and 180-190. Electrostatic interactions could distinctly influence on the binding specificity and affinity of a protein with substrates. This unique charge distribution is most likely to have a profound effect on the ability of RaPrP^C to interact with other molecules.

The S173N substitution causes marked changes in the surface charge distribution for RaPrP^C. RaPrP^C-(91-228) displays a neutral charge distribution around the position of residue 173, while the S173N variant carries negative charge in the same position (Fig. 3, A and B). Surface charge changes are observed not only in the right substituted position but also at other sites such as residue Q219, from negative charge in the wild-type to neutral charge in the variant (Fig. 3, C and D). A discontinuous epitope of residues 167, 171, 214 and 218 has been suggested to be involved in the binding of PrP^C with the putative protein X (40). Misfolding and propagation of the prion protein mediated by protein X is likely to occur if the surface-restricted electrostatic potential would not work as a barrier for intermolecular interactions.

Hydrogen bonding networks- Hydrogen bonds usually have important roles in stabilizing tertiary structures. We compared the hydrogen bonding networks between the wild-type RaPrP^C-(91-228) and the S173N variant. As a criterion, hydrogen bonds are thought to be stable if they exist in at least 9 structures among the 15 lowest-energy structures. Totally, 55 hydrogen bonds are detected in the wild-type, however, only 47 in the variant, implying that the S173N substitution decreases the structural stability. A set of hydrogen bonds, which make significant contribution to maintain the tertiary structure for either the wild-type or the variant, are listed in Table 2. The distribution and number of hydrogen bonds in RaPrP^C-(91-228) is dramatically different from that of the S173N variant (Table 2). Therefore, it could be expected that the structural change in the S173N variant is more or less readily to be induced by other chaperones.

Conformational stability- To evaluate the effect of the S173N substitution on the conformational stability, we measured the urea-induced unfolding transitions of both RaPrP^C-(121-228) and the S173N variant using CD spectroscopy (Fig. 4). Far-UV CD spectra show the change of secondary structure with the increase of urea concentration (Fig. 4, A and B). Due to irreversible denaturation for either the wild-type or the variant (Supplemental Fig. S2, A and B), we determined the apparent thermodynamic parameters for the equilibrium unfolding. Both the apparent free energy $\Delta G_{N\to U}^{H_2O}$ and the midpoint denaturant concentration C_m are lessened after the S173N substitution (Table 3), suggesting that the conformational stability of the S173N variant is decreased compared to that of the wild-type. The coefficient m, which is linked to the solvent accessible surface area and hydrophobic interactions (43-46), is also significantly altered with the S173N exchange (Table 3), indicative of distinct difference in hydrophobic interactions between the wild-type and the variant.

Near-UV CD spectra reflect the change of tertiary structure against urea concentration (Fig. 4, C and D). Both the wild-type and the S173N variant show the minimal values at 268 nm, thus the mean residue ellipticity (θ) at this wavelength is selected for analysis. The trends of θ_{268} are coincident with theoretical sigmoid curves, similar to those of θ_{222}. The midpoint C_m values are

approximately 5.3 M for the wild-type and 4.9 M for the S173N variant, implying a lower conformational stability after the S173N substitution. The C_m values in the near-UV CD spectra are much smaller than the corresponding values in the far-UV CD spectra (Fig. 4 and Table 3), which suggests that the change of tertiary structure is prior to that of secondary structure for the two proteins upon urea denaturation. For a higher urea concentration, however, the change of secondary and tertiary structures occurs simultaneously.

Relaxation rates R_1, R_2 and {^{1}H}-^{15}N heteronuclear NOE of RaPrP^C-(121-228)- A complete description of the tertiary structure of a protein requires a well understanding of how the structure changes with time. The measurement of ^{15}N spin relaxation parameters for N-H bond vectors provides valuable information about internal dynamics of proteins on both pico- to nanosecond and micro- to millisecond time scales (47,48). Recent work has demonstrated that changes in motions can influence protein functions even if conformations are the same (49). To gain an insight into the backbone dynamics of RaPrP^C-(121-228) in solution, we measured ^{15}N longitudinal (T_1), transverse (T_2) relaxation times and {^{1}H}-^{15}N heteronuclear NOEs. Totally, 97 N-H resonances were assigned and used in the dynamics analysis for RaPrP^C-(121-228). We utilized peak height to represent peak intensity so that the disturbance of partially overlapping peaks could be eliminated. Relaxation rates R_1, R_2 and {^{1}H}-^{15}N heteronuclear NOE values versus the residue number are shown in Fig. 5A. The measured R_1 rates range from 1.0 s^{-1} to 1.6 s^{-1} with a mean value of 1.28 s^{-1} approximately. R_1 values of residues in helix3 are smaller than those in the other two helices. R_2 rates show a relatively variable profile ranging from 3.4 s^{-1} to 20.5 s^{-1} with an average value of around 13.4 s^{-1}. The mean R_2 values for residues in helices 1, 2 and 3 are 13.43, 14.87 and 15.87 s^{-1}, respectively. Lower R_2 values are observed in residues 121-126 and 189-197. Interestingly, D166 exhibits the largest R_2 value higher than 20 s^{-1}. Furthermore, G130 also shows a larger R_2 value compared to those of its neighboring residues. All the NOE values are positive except those of the first two residues. NOE values for residues in secondary structure regions are distinctly higher than those in loop fragments such as residues 121-126 and 189-197, similar to the R_2 distribution. Residues involved in α-helix or β-strand structural elements possess NOE values larger than 0.65, indicative of more restricted dynamics in these regions.

Reduced spectral density functions $J(\omega_N)$, $J(0)$ and $J(0.87\omega_H)$ of RaPrP^C-(121-228)- We adopted the spectral density function approach (28-30) to interpret the relaxation data. The calculated values of reduced spectral density functions $J(\omega_N)$, $J(0)$ and $J(0.87\omega_H)$ versus the residue number for RaPrP^C-(121-228) are plotted in Fig. 6A. The $J(\omega_N)$ value shows less variation with the residue number, with typical values between 0.25 and 0.36 ns·rad^{-1}. The average value for helix-3 is 0.29 ns·rad^{-1}, lower than 0.33 ns·rad^{-1} for helix-1 or 0.32 ns·rad^{-1} for helix-2. Residues in both helix-3 and loop 131-140 exhibit smaller contributions to $J(\omega_N)$.

The low frequency spectral density function $J(0)$ covers a wide range of values from 1.0 ns·rad^{-1} to 7.5 ns·rad^{-1}, with a mean value of 4.8 ns·rad^{-1} approximately. The smaller the $J(0)$ value, the greater the sub-nanosecond flexibility of the N-H bond vector (50). Three loop regions, including residues 121-126, 138-141 and 190-198, show very low $J(0)$ values, implicating the internal flexibility of the N-H bonds. Unexpectedly, H186 in helix-2 also exhibits a fairly small $J(0)$ value, indicative of the sub-nanosecond flexibility. $J(0)$ values for secondary structural elements are relatively higher, indicating that these well-structured regions possess limited internal mobility. Slow micro- to millisecond motions (R_{ex}) are usually reflected as significant increases in $J(0)$ values (51-53). D166 has the highest $J(0)$ value of around 7.5 ns·rad^{-1}, implying a slow R_{ex} motion. G130 in β-strand S1 shows a distinctly large $J(0)$ value without any notable feature in either the $J(\omega_N)$ or $J(0.87\omega_H)$ value, implicating a significant contribution from the slow R_{ex} motion. Residues with marked R_{ex} motions are likely to be involved in some important biological events, for example, interactions with other molecules *in vivo*.

The high frequency spectral density function $J(0.87\omega_H)$ has relatively small values ranging from 0.002 ns·rad^{-1} to 0.03 ns·rad^{-1}. The distribution of $J(0.87\omega_H)$ values, with larger values in loop fragments and smaller values in structured regions, is opposite to that of $J(0)$ values. Large $J(0.87\omega_H)$

values are observed for residues 121-126, 189-197 and H186, suggesting these N-H bonds experience fast picosecond motions. There are no significant differences in low $J(0.87\omega_H)$ values for most residues in helices 1, 2 and 3, which indicates that these three helices are subjected to little internal motions on fast picosecond time scale.

Order parameters S^2 of RaPrP^C-(121-228)- The modelfree formalism is usually used to analyze internal motions of a protein (32-34). The $D_{//}/D_{\perp}$ ratio of the rotational diffusion tensor of RaPrP^C-(121-228) is calculated to be 1.31 ± 0.01 using the r2r1_diffusion program (kindly provided by Prof. A.G. Palmer Ⅲ), suggesting that the axially symmetric model is suitable for the data fitting. We determined the order parameter S^2 for each residue in RaPrP^C-(121-228) (Fig. 7A). The order parameter quantitatively describes the amplitude of the internal motion on nanosecond time scale. Residues with S^2 lower than 0.7 are mostly observed in three flexible loop fragments including residues 121-126, 138-141 and 190-198. However, loop 165-172, which connects β-sheet-2 and α-helix-2, exhibits large S^2 values over 0.85, indicating a highly ordered loop. Residues in secondary structure elements have relatively higher S^2, typically with values larger than 0.8, indicative of rigid regions with restricted internal motions. The mean S^2 values for residues in helices 1, 2 and 3 are 0.93, 0.94 and 0.85, respectively. The S^2 values are mapped onto the tertiary structure of RaPrP^C and shown in Fig. 7C.

Backbone dynamics of the S173N variant- To investigate whether the S173N substitution would influence the internal motions of the RaPrP^C molecule, we analyzed the backbone dynamics of the structured C-terminal domain-(121-228) of the S173N variant. The overall distributions of relaxation parameters (Fig. 5B) and the reduced spectral density functions (Fig. 6B) for the S173N variant are similar to those for the wild-type. The value differences of the reduced spectral densities for two local regions, including loop 165-172 and the half end of helix-3, between the wild-type and the S173N variant are shown in Fig. 6C. Increased internal flexibility usually causes a decrease of the $J(\omega_N)$ value for small proteins (50,54). Greater sub-nanosecond flexibility can be also reflected in smaller $J(0)$ values (50). Unlike insignificant changes in $\triangle J(0.87\omega_H)$, most of the residues in loop 165-172 and at the half end of helix-3 exhibit positive values in $\triangle J(\omega_N)$ and $\triangle J(0)$ (Fig. 6C), implicating more internal mobility of the two regions in the S173N variant. Thus, the S173N substitution potentially disturbs the interaction between loop 165-172 and helix-3. Furthermore, as the $D_{//}/D_{\perp}$ ratio of the rotational diffusion tensor of the variant is 1.46 ± 0.01, we selected the axially symmetric model for the modelfree analysis. We determined order parameters S^2 (Fig. 7B) and mapped them onto the tertiary structure of the S173N variant (Fig. 7D). Unexpectedly, the end of helix-3 in the variant exhibits S^2 values lower than 0.8 (Fig. 7B), dramatically smaller than those of the corresponding residues in the wild-type (Fig. 7), suggesting that the S173N substitution significantly increases structural flexibility. Usually, the local region of high flexibility is associated with a lower energy barrier to structural rearrangement. Therefore, the conformational rigidity of RaPrP^C may allow this protein to resist to the induction of other molecules and successfully escape from the conformational conversion.

Discussion

Rabbits are among the few mammalian species that are capable of surviving with the infection of TSE agents due to some unique structural characteristics of the RaPrP^C molecule itself (19). In this present work, we determined the solution structures of the recombinant protein RaPrP^C-(91-228) and its S173N variant, and detected the backbone dynamics of their globular structured C-terminal domains-(121-228). Kurt Wuthrich group have proved that the three-dimensional structure of the labeled recombinant bPrP^C is identical to that of the unlabeled natural glycoprotein isolated from calf brains (13,55), which provides solid evidence that isotopic labeling used in bio-NMR does not effect the conformation of the protein. Our results also show that the conformations of labeled or unlabeled RaPrP^{C}s are essentially identical (Supplemental Fig. S3, A and B). Thus the tertiary structure presented here represents the true conformation of the RaPrP^C molecule. Previous studies have revealed that the homologous loop 165-172 is related to prion diseases (56,57). NMR resonances in loop 165-172 are unobservable for many mammalian PrP^{C}s such as mPrP^C, hPrP^C or

bPrP^C (10,12,13). Only a few mammalian PrP^{C}s, including elk PrP^C (ePrP^C), Tammar wallaby PrP^C (twPrP^C) and horse PrP^C (ecPrP^C) (15,16,58) have not missed resonances. Loop 165-172 in RaPrP^C can be well assigned by long-range NOEs from the residues at the end of helix-3. Recently, the modelfree approach has been successfully employed to elucidate the backbone dynamics for mPrP^C-(121-230) (59). Nevertheless, order parameters S^2 for the corresponding loop in mPrP^C are not available due to invisible backbone resonances. We have demonstrated that the well-defined loop 165-172 in RaPrP^C is highly ordered, supported by the S^2 values measured for the first time, providing an important insight into the species barrier of the infection of TSEs. The S173N exchange does not influence the overall scaffold of the RaPrP^C molecule, however, the urea-induced transition experiments have illustrated a decrease in global conformational stability after the substitution. Molecular dynamics (MD) simulations do not find the difference of PrP^C stability among species (60), but confirm the structural stability of the wild-type RaPrP^C compared with the variants and show that the salt bridge between D177 and R163 makes a great contribution (61). Such a salt bridge, however, is not observed in our work possibly owing to the low pH condition. Our results have indicated that the decreased conformational stability after the S173 substitution is relevant to distinct changes of hydrogen bonding networks and hydrophobic interactions. In particular, the S173N substitution causes an increase in structural flexibility of loop 165-172 and the end of helix-3, implying an alteration in the interaction of loop 165-172 with helix-3. The interaction between these two regions is implicated to have a crucial role in stabilization of the PrP^C structure (62). Previous studies demonstrate that helix-1 is rather stable against environmental perturbations and unlikely to be involved in the initial steps of the pathogenic conformational change (63,64). Recent reports show that helix-2 and helix-3 in the structured C-terminal domain of the PrP^C protein are most likely to undergo a transition to β-structure (65-67). Therefore, the highly ordered loop 165-172 and its interaction with helix-3 may form a huge barrier to prevent the C-terminal domain of RaPrP^C from the conformational conversion. Barbara Christen et al. have inferred that the interaction between these two conformational markers could act as regulators of the functional specificity of PrP^C (15). The study reported by Andrew F. Hill group suggests that the rabbit-specific residues surrounding the C-terminal GPI anchor may interfere with a PrP^{Sc} interaction site (68).

It is unlikely for PrP^C to undergo a spontaneous transition without any induction of the chaperone in the complicated cellular environment. Previous studies have suggested that PrP^{Sc}, protein X and specific nucleic acid could bind to PrP^C and induce conformational changes (2,39,40,69-71). The surface charge distributions around binding sites usually have important roles in determining the binding specificities of proteins with substrates (72,73). One single residue change can lead to significant influences on the surface charge distribution of a protein such as the S173N variant of RaPrP^C described herein and the E200K variant of hPrP^C reported by Zhang et al (41). The distribution of electrostatic potential for RaPrP^C, with a large area of continuous positive charge on the surface, is dramatically different from those of other PrP^{C}s, which would make significant contribution to protect RaPrP^C from the conformational conversion. PrP^{Sc} has been identified as the infectious agent of TSEs. Transgenetic studies indicate that the formation of PrP^{Sc} requires the PrP^C substrate to bind to the PrP^{Sc} product at an intermediate stage of the conformational conversion process (69). PrP^{Sc} could recognize the surface of PrP^C containing fragments 90-144 and 180-205 (2). The area of continuous positive charge on the surface of RaPrP^C roughly covers residues 125-135, 150-160 and 180-190. Thus, the interaction of PrP^C with PrP^{Sc} is likely to be inhibited due to the exclusive distribution of electrostatic potential on the surface of RaPrP^C. In addition, much evidence supports the hypothesis that the conformational conversion of PrP^C into PrP^{Sc} is a key molecular event for the pathogenesis of TSEs (74-77). Both DNA and RNA may stimulate the misfolding process of prions (70,71). Recent studies have reported that the DNA-PrP^C interaction is mediated mainly through the globular structured domain of PrP^C, with a recruitment of residues in the N-terminal unstructured loop 91-120 (78,79). Electrostatic contacts are one of the most important factors for DNA or RNA recognition by proteins. The unique surface charge distribution of RaPrP^C, especially

the continuous positive-charged region contained in the globular C-terminal domain, may significantly influence the electrostatic interaction of $RaPrP^C$ with the specific nucleic acid. The distinct nucleic acid-$RaPrP^C$ interaction potentially leads to the inability of $RaPrP^C$ to undergo the conformational transition.

The partially exposed residue H186 has been demonstrated to be able to disrupt the surrounding hydrophobic interactions upon protonation at acidic pH, resulting in destabilization of the C-terminal half of helix-2 (59). H186 is also involved in the copper (Ⅱ) binding (80,81), which may cause a decrease in the structural stability of helix-2. On the other hand, PrP^{Sc} could recognize a surface area of PrP^C containing fragments 90-144 and 180-205 (2). Destabilization of PrP^C is required for the interaction of PrP^C with PrP^{Sc} *in vitro* (82-84). In addition, Our NMR dynamics analysis shows that H186 undergoes significant internal motions although it is located in a secondary structure element (helix-2). Thus, the residue H186 is expected to act as a trigger for the initial binding of PrP^C to PrP^{Sc}. However, only this step may be not sufficient for the conformational conversion of prions since $RaPrP^C$ is not yet converted to the proteinase-resistant form in Sc^+-MNB cells (19). We thus suggest that the highly ordered loop 165-172 and its interaction with helix-3, together with the unique distribution of surface electrostatic potential, significantly contribute to the unique structural characteristics of $RaPrP^C$. Our results will be helpful to understand the underlying molecular mechanism of the conformational conversion for prion proteins.

References

1. Prusiner, S. B. (1982) *Science* **216**, 136-144
2. Prusiner, S. B. (1998) *Proc Natl Acad Sci U S A* **95**, 13363-13383
3. Stahl, N., Baldwin, M. A., Teplow, D. B., Hood, L., Gibson, B. W., Burlingame, A. L., and Prusiner, S. B. (1993) *Biochemistry* **32**, 1991-2002
4. Caughey, B. W., Dong, A., Bhat, K. S., Ernst, D., Hayes, S. F., and Caughey, W. S. (1991) *Biochemistry* **30**, 7672-7680
5. Pan, K. M., Baldwin, M., Nguyen, J., Gasset, M., Serban, A., Groth, D., Mehlhorn, I., Huang, Z., Fletterick, R. J., Cohen, F. E., and Prusiner, S. B. (1993) *Proc Natl Acad Sci U S A* **90**, 10962-10966
6. Pauly, P. C., and Harris, D. A. (1998) *J Biol Chem* **273**, 33107-33110
7. Brown, D. R., Wong, B. S., Hafiz, F., Clive, C., Haswell, S. J., and Jones, I. M. (1999) *Biochem J* **344**, 1-5
8. Vassallo, N., and Herms, J. (2003) *J Neurochem* **86**, 538-544
9. Lauren, J., Gimbel, D. A., Nygaard, H. B., Gilbert, J. W., and Strittmatter, S. M. (2009) *Nature* **457**, 1128-1132
10. Riek, R., Hornemann, S., Wider, G., Billeter, M., Glockshuber, R., and Wuthrich, K. (1996) *Nature* **382**, 180-182
11. Donne, D. G., Viles, J. H., Groth, D., Mehlhorn, I., James, T. L., Cohen, F. E., Prusiner, S. B., Wright, P. E., and Dyson, H. J. (1997) *Proc Natl Acad Sci U S A* **94**, 13452-13457
12. Zahn, R., Liu, A., Luhrs, T., Riek, R., von Schroetter, C., Lopez Garcia, F., Billeter, M., Calzolai, L., Wider, G., and Wuthrich, K. (2000) *Proc Natl Acad Sci U S A* **97**, 145-150
13. Lopez Garcia, F., Zahn, R., Riek, R., and Wuthrich, K. (2000) *Proc Natl Acad Sci U S A* **97**, 8334-8339
14. Lysek, D. A., Schorn, C., Nivon, L. G., Esteve-Moya, V., Christen, B., Calzolai, L., von Schroetter, C., Fiorito, F., Herrmann, T., Guntert, P., and Wuthrich, K. (2005) *Proc Natl Acad Sci U S A* **102**, 640-645
15. Christen, B., Hornemann, S., Damberger, F. F., and Wuthrich, K. (2009) *J Mol Biol* **389**, 833-845
16. Perez, D. R., Damberger, F. F., and Wuthrich, K. (2010) *J Mol Biol* **400**, 121-128
17. Calzolai, L., Lysek, D. A., Guntert, P., von Schroetter, C., Riek, R., Zahn, R., and Wuthrich, K. (2000) *Proc Natl Acad Sci U S A* **97**, 8340-8345
18. Gibbs, C. J., Jr., and Gajdusek, D. C. (1973) *Science* **182**, 67-68
19. Vorberg, I., Groschup, M. H., Pfaff, E., and Priola, S. A. (2003) *J Virol* **77**, 2003-2009
20. Yin, S. M., Zheng, Y., and Tien, P. (2003) *Protein Expr Purif* **32**, 104-109
21. Delaglio, F., Grzesiek, S., Vuister, G. W., Zhu, G., Pfeifer, J., and Bax, A. (1995) *J Biomol NMR* **6**, 277-293
22. Li, J., Mei, F. H., Xiao, G. F., Guo, C. Y., and Lin, D. H. (2007) *J Biomol NMR* **38**, 181
23. Nilges, M., Macias, M. J., O'Donoghue, S. I., and Oschkinat, H. (1997) *J Mol Biol* **269**, 408-422
24. Brunger, A. T., Adams, P. D., Clore, G. M., DeLano, W. L., Gros, P., Grosse-Kunstleve, R. W., Jiang, J. S., Kuszewski, J., Nilges, M., Pannu, N. S., Read, R. J., Rice, L. M., Simonson, T., and Warren, G. L. (1998)

Acta Crystallogr D Biol Crystallogr **54**, 905-921
25. Laskowski, R. A., Rullmannn, J. A., MacArthur, M. W., Kaptein, R., and Thornton, J. M. (1996) *J Biomol NMR* **8**, 477-486
26. Koradi, R., Billeter, M., and Wuthrich, K. (1996) *J Mol Graph* **14**, 51-55, 29-32
27. Farrow, N. A., Muhandiram, R., Singer, A. U., Pascal, S. M., Kay, C. M., Gish, G., Shoelson, S. E., Pawson, T., Forman-Kay, J. D., and Kay, L. E. (1994) *Biochemistry* **33**, 5984-6003
28. Peng, J. W., and Wagner, G. (1992) *Biochemistry* **31**, 8571-8586
29. Peng, J. W., and Wagner, G. (1992) *J Magn Reson* **98**, 308-332
30. Farrow, N. A., Zhang, O., Szabo, A., Torchia, D. A., and Kay, L. E. (1995) *J Biomol NMR* **6**, 153-162
31. Spyracopoulos, L. (2006) *J Biomol NMR* **36**, 215-224
32. Lipari, G., and Szabo, A. (1982) *J Am Chem Soc* **104**, 4546-4559
33. Lipari, G., and Szabo, A. (1982) *J Am Chem Soc* **104**, 4559-4570
34. Clore, G. M., Szabo, A., Bax, A., Kay, L. E., Driscoll, P. C., and Gronenborn, A. (1990) *J Am Chem Soc* **112**, 4989-4991
35. Barbato, G., Ikura, M., Kay, L. E., Pastor, R. W., and Bax, A. (1992) *Biochemistry* **31**, 5269-5278
36. Cole, R., and Loria, J. P. (2003) *J Biomol NMR* **26**, 203-213
37. Bolen, D. W., and Santoro, M. M. (1988) *Biochemistry* **27**, 8069-8074
38. Santoro, M. M., and Bolen, D. W. (1988) *Biochemistry* **27**, 8063-8068
39. Telling, G. C., Scott, M., Mastrianni, J., Gabizon, R., Torchia, M., Cohen, F. E., DeArmond, S. J., and Prusiner, S. B. (1995) *Cell* **83**, 79-90
40. Kaneko, K., Zulianello, L., Scott, M., Cooper, C. M., Wallace, A. C., James, T. L., Cohen, F. E., and Prusiner, S. B. (1997) *Proc Natl Acad Sci U S A* **94**, 10069-10074
41. Zhang, Y., Swietnicki, W., Zagorski, M. G., Surewicz, W. K., and Sonnichsen, F. D. (2000) *J Biol Chem* **275**, 33650-33654
42. Billeter, M., Riek, R., Wider, G., Hornemann, S., Glockshuber, R., and Wuthrich, K. (1997) *Proc Natl Acad Sci U S A* **94**, 7281-7285
43. Privalov, P. L., and Makhatadze, G. I. (1990) *J Mol Biol* **213**, 385-391
44. Alonso, D. O., and Dill, K. A. (1991) *Biochemistry* **30**, 5974-5985
45. Dill, K. A., and Shortle, D. (1991) *Annu Rev Biochem* **60**, 795-825
46. Privalov, P. L., and Makhatadze, G. I. (1992) *J Mol Biol* **224**, 715-723
47. Kay, L. E. (1998) *Nat Struct Biol* **5 Suppl**, 513-517
48. Dyson, H. J., and Wright, P. E. (2001) *Methods Enzymol* **339**, 258-270
49. Tzeng, S. R., and Kalodimos, C. G. (2009) *Nature* **462**, 368-372
50. Lefevre, J. F., Dayie, K. T., Peng, J. W., and Wagner, G. (1996) *Biochemistry* **35**, 2674-2686
51. Viles, J. H., Donne, D., Kroon, G., Prusiner, S. B., Cohen, F. E., Dyson, H. J., and Wright, P. E. (2001) *Biochemistry* **40**, 2743-2753
52. Dyson, H. J., and Wright, P. E. (2002) *Adv Protein Chem* **62**, 311-340
53. O'Sullivan, D. B., Jones, C. E., Abdelraheim, S. R., Brazier, M. W., Toms, H., Brown, D. R., and Viles, J. H. (2009) *Protein Sci* **18**, 410-423
54. Dayie, K. T., Wagner, G., and Lefevre, J. F. (1996) *Annu Rev Phys Chem* **47**, 243-282
55. Hornemann, S., Schorn, C., and Wuthrich, K. (2004) *EMBO Rep* **5**, 1159-1164
56. Sigurdson, C. J., and Aguzzi, A. (2007) *Biochim Biophys Acta* **1772**, 610-618
57. Christen, B., Perez, D. R., Hornemann, S., and Wuthrich, K. (2008) *J Mol Biol* **383**, 306-312
58. Gossert, A. D., Bonjour, S., Lysek, D. A., Fiorito, F., and Wuthrich, K. (2005) *Proc Natl Acad Sci U S A* **102**, 646-650
59. Bae, S. H., Legname, G., Serban, A., Prusiner, S. B., Wright, P. E., and Dyson, H. J. (2009) *Biochemistry* **48**, 8120-8128
60. Zhang, J. (2009) *J Biomol Struct Dyn* **27**, 159-162
61. Zhang, J. (2010) *J Theor Biol* **264**, 119-122
62. James, T. L., Liu, H., Ulyanov, N. B., Farr-Jones, S., Zhang, H., Donne, D. G., Kaneko, K., Groth, D., Mehlhorn, I., Prusiner, S. B., and Cohen, F. E. (1997) *Proc Natl Acad Sci U S A* **94**, 10086-10091
63. Ziegler, J., Sticht, H., Marx, U. C., Muller, W., Rosch, P., and Schwarzinger, S. (2003) *J Biol Chem* **278**, 50175-50181
64. Santini, S., and Derreumaux, P. (2004) *Cell Mol Life Sci* **61**, 951-960
65. Dima, R. I., and Thirumalai, D. (2004) *Proc Natl Acad Sci U S A* **101**, 15335-15340
66. Cobb, N. J., Sonnichsen, F. D., McHaourab, H., and Surewicz, W. K. (2007) *Proc Natl Acad Sci U S A* **104**,

18946-18951
67. Lu, X., Wintrode, P. L., and Surewicz, W. K. (2007) *Proc Natl Acad Sci U S A* **104**, 1510-1515
68. Nisbet, R. M., Harrison, C. F., Lawson, V. A., Masters, C. L., Cappai, R., and Hill, A. F. (2010) *J Virol* **84**, 6678-6686
69. Prusiner, S. B., Scott, M., Foster, D., Pan, K. M., Groth, D., Mirenda, C., Torchia, M., Yang, S. L., Serban, D., Carlson, G. A., Hoppe, P. C., Westaway, D., and DeArmond, S. J. (1990) *Cell* **63**, 673-686
70. Cordeiro, Y., Machado, F., Juliano, L., Juliano, M. A., Brentani, R. R., Foguel, D., and Silva, J. L. (2001) *J Biol Chem* **276**, 49400-49409
71. Deleault, N. R., Lucassen, R. W., and Supattapone, S. (2003) *Nature* **425**, 717-720
72. Zhang, M., Stauffacher, C. V., Lin, D., and Van Etten, R. L. (1998) *J Biol Chem* **273**, 21714-21720
73. Xu, H., Xia, B., and Jin, C. (2006) *J Bacteriol* **188**, 1509-1517
74. Legname, G., Baskakov, I. V., Nguyen, H. O., Riesner, D., Cohen, F. E., DeArmond, S. J., and Prusiner, S. B. (2004) *Science* **305**, 673-676
75. Castilla, J., Saa, P., Hetz, C., and Soto, C. (2005) *Cell* **121**, 195-206
76. Surewicz, W. K., Jones, E. M., and Apetri, A. C. (2006) *Acc Chem Res* **39**, 654-662
77. Wang, F., Wang, X., Yuan, C. G., and Ma, J. (2010) *Science* **327**, 1132-1135
78. Lima, L. M., Cordeiro, Y., Tinoco, L. W., Marques, A. F., Oliveira, C. L., Sampath, S., Kodali, R., Choi, G., Foguel, D., Torriani, I., Caughey, B., and Silva, J. L. (2006) *Biochemistry* **45**, 9180-9187
79. Tjong, H., and Zhou, H. X. (2007) *Nucleic Acids Res* **35**, 1465-1477
80. Colombo, M. C., Vandevondele, J., Van Doorslaer, S., Laio, A., Guidoni, L., and Rothlisberger, U. (2008) *Proteins* **70**, 1084-1098
81. Zidar, J., Pirc, E. T., Hodoscek, M., and Bukovec, P. (2008) *J Chem Inf Model* **48**, 283-287
82. Kocisko, D. A., Come, J. H., Priola, S. A., Chesebro, B., Raymond, G. J., Lansbury, P. T., and Caughey, B. (1994) *Nature* **370**, 471-474
83. Kaneko, K., Peretz, D., Pan, K. M., Blochberger, T. C., Wille, H., Gabizon, R., Griffith, O. H., Cohen, F. E., Baldwin, M. A., and Prusiner, S. B. (1995) *Proc Natl Acad Sci U S A* **92**, 11160-11164
84. Kaneko, K., Wille, H., Mehlhorn, I., Zhang, H., Ball, H., Cohen, F. E., Baldwin, M. A., and Prusiner, S. B. (1997) *J Mol Biol* **270**, 574-586

Footnotes

We would like to thank Prof. Daiwen Yang (National University of Singapore) for helpful discussions on dynamics analysis. This work was supported by grants from the National Natural Science Foundation of China (Nos. 30730026, 30570352) and National Science & Technology Major Project "Key New Drug Creation and Manufacturing Program"，China (No. 2009ZX09301-001).

† These authors contributed equally to this work.

§Present address: Jun Li, Department of Structural Biology, University of Pittsburgh School of Medicine, Pittsburgh, Pennsylvania 15260, USA.

Abbreviations used: PrP^{C}, cellular isoform of prion protein; PrP^{Sc}, scrapie isoform of prion protein; $RaPrP^{C}$, rabbit PrP^{C}; $mPrP^{C}$, mouse PrP^{C}; $hPrP^{C}$, human PrP^{C}; $ShPrP^{C}$, Syrian hamster PrP^{C}; $bPrP^{C}$, bovine PrP^{C}; $ePrP^{C}$, elk PrP^{C}; $twPrP^{C}$, Tammar wallaby PrP^{C}; $ecPrP^{C}$, horse PrP^{C}; TSE, transmissible spongiform encephalopathy; BSE, bovine spongiform encephalopathy; CJD, Creutzfeldt-Jakob disease; GdnHCl, guanidinium chloride; GPI, glycosylphosphatidylinositol.

Figure legends

Fig. 1. Solution structures of wild-type $RaPrP^{C}$-(91-228) and its S173N variant. Backbone superposition of the 15 lowest-energy conformers representing the solution structures of (A) the wild-type and (C) the variant. Ribbon diagram of the mean structures of (B) the wild-type and (D) the variant showing the secondary structure elements. These structures were determined in 20 mM sodium acetate buffer at pH 4.5.

Fig. 2. Distributions of electrostatic potential of (A) $RaPrP^{C}$ (PDB code: 2FJ3) or (B) $hPrP^{C}$ (PDB code: 1QM3) or (C) $mPrP^{C}$ (PDB code: 1XYX) or (D) $bPrP^{C}$ (PDB code: 1DWZ). Three-dimensional structures of these PrP^{C}s were all determined in sodium acetate buffer at pH 4.5. Blue for positive charge whereas

red for negative charge. The surface graphs are generated using MolMol.

Fig. 3. The surface charge distributions of wild-type RaPrP^{C}-(91-228) and the S173N variant. Position 173 of (A) the wild-type and (B) the variant. Position 219 of (C) the wild-type and (D) the variant. Blue for positive charge whereas red for negative charge. The surface graphs are generated using MolMol.

Fig. 4. Urea-induced unfolding transitions of wild-type RaPrP^{C}-(121-228) and the S173N variant measured by CD at 25 ℃. Far-UV CD spectra of (A) the wild-type and (B) the variant. The sample concentration is approximately 0.2 mg·ml^{-1}. The mean residue ellipticity at 222 nm versus the urea concentration is ploted. The inserts show the change of secondary structures induced by urea from 4.5 M to 9 M with an increment of 0.5 M, together with dashed lines reflecting secondary structures in the absence of urea. Near-UV CD spectra of (C) the wild-type and (D) the variant. The sample concentration is 1 mg·ml^{-1}. The mean residue ellipticity at 268 nm is analyzed. The inserts show the change of tertiary structures against urea concentration from 3 M to 8.5 M with an increment of 0.5 M, together with dashed lines representing tertiary structures without urea.

Fig. 5. Relaxation rates R_1, R_2 and $\{^1H\}$-^{15}N heteronuclear NOEs of (A) RaPrP^{C}-(121-228) and (B) the S173N variant. The regular secondary structure elements are indicated on the top. The experiments were performed at 25 ℃ on a Varian Unity Inova 600 MHz spectrometer. The sample was dissolved in Buffer F (20 mM NaAc, 0.02% NaN_3, pH 4.5).

Fig. 6. Reduced spectral density functions of wild-type RaPrP^{C}-(121-228) and the S173N variant. $J(\omega_N)$, $J(0)$ and $J(0.87\omega_H)$ of (A) the wild-type and (B) the S173N variant. (C) Differences of spectral densities for residues in loop 165-172 and at the C-terminal half of helix-3 between the wild-type and the S173N variant. The difference is calculated as follows: $\triangle J(\omega)=J(\omega)_{\text{wild-type}}-J(\omega)_{\text{variant}}$. The regular secondary structure elements are indicated on the top.

Fig. 7. Order parameters S^2 for (A) RaPrP^{C}-(121-228) and (B) the S173N variant. The regular secondary structure elements are indicated on the top. S^2 values are mapped onto the tertiary structures of (C) RaPrP^{C}-(121-228) and (D) the S173N variant: red for $S^2 < 0.6$, orange for $0.6 \leq S^2 < 0.7$, yellow for $0.7 \leq S^2 < 0.8$, green for $0.8 \leq S^2 < 0.9$, blue for $0.9 \leq S^2 < 1.0$, and grey for S^2 unavailable due to the absence of data or failure in data fitting. The ribbon graphs are generated using PyMol.

Table 1. Structural statistics of RaPrP^{C}-(91-228) and the S173N variant

Quantity	Value	
	RaPrP^{C}-(91-228)	S173N
Distance restraints		
Intraresidue (| i-j | = 0)	911	788
Sequential (| i-j | = 1)	672	712
Medium range (2 < | i-j | < 4)	578	655
Long range (| i-j | > 5)	684	808
Total	2845	2963
Dihedral angle restraints (Φ and Ψ)[a]	134	134
Hydrogen bond restraints	54	54
Restraints violations (15 structures)		
NOE distance violation (> 0.3 Å)	0	0
Torsion angle violation (> 5°)	0	0
RMSD from mean structure (Å)		
All residues (backbone)	0.78 ± 0.16	0.85 ± 0.28
Secondary structures (backbone)	0.60 ± 0.15	0.53 ± 0.15
All residues (heavy atoms)	1.44 ± 0.22	1.51 ± 0.30
Secondary structures (heavy atoms)	1.29 ± 0.21	1.28 ± 0.21
Ramachandran analysis (%) (124-228)[b]		
Residues in most favored regions	78.9	77.0
Residues in additionally allowed regions	14.7	17.4
Residues in generously allowed regions	5.3	5.3
Residues in disallowed regions	1.1	0.3

[a] The dihedral angle restraints are generated from secondary structure by CSI.
[b] Residues included in analysis are indicated in parentheses.

Table 2. Hydrogen bonds maintaining the tertiary structures of $RaPrP^{C}$-(91-228) and the S173N variant

Protein	Hydrogen bonds
$RaPrP^{C}$-(91-228)	$M128H^{N}$-Y162O, $G130H^{N}$-V160O, $I138H^{N}$-Y149O, R155HH12-D201OD1, R155HH22-Y148O, H176HD1-E210OE2, H186HD1-R155O, S221HG-D166OD1
S173N	H139HD1-D146OD1, $Y161H^{N}$-T182OG1, $Y162H^{N}$-M128O, T182HG1-Q159O

Table 3. Apparent thermodynamic parameters for the equilibrium unfolding of RaPrP^{C}-(121-228) and the S173N variant at 25 ℃. $\Delta G_{N\to U}^{H_2O}$ is an estimate of the free energy in the absence of denaturant, the parameter m represents the cooperativity of the unfolding transition, and C_m is the concentration of urea at the midpoint of unfolding.

Protein	$\Delta G_{N\to U}^{H_2O}$ (kJ·mol^{-1})	m (kJ·mol^{-1}·M^{-1})	C_m (M)
RaPrP^{C}-(121-228)	26.2 ± 2.7	-3.88 ± 0.49	6.49 ± 0.05
S173N	16.0 ± 1.6	-2.52 ± 0.35	6.04 ± 0.06

Figure 1

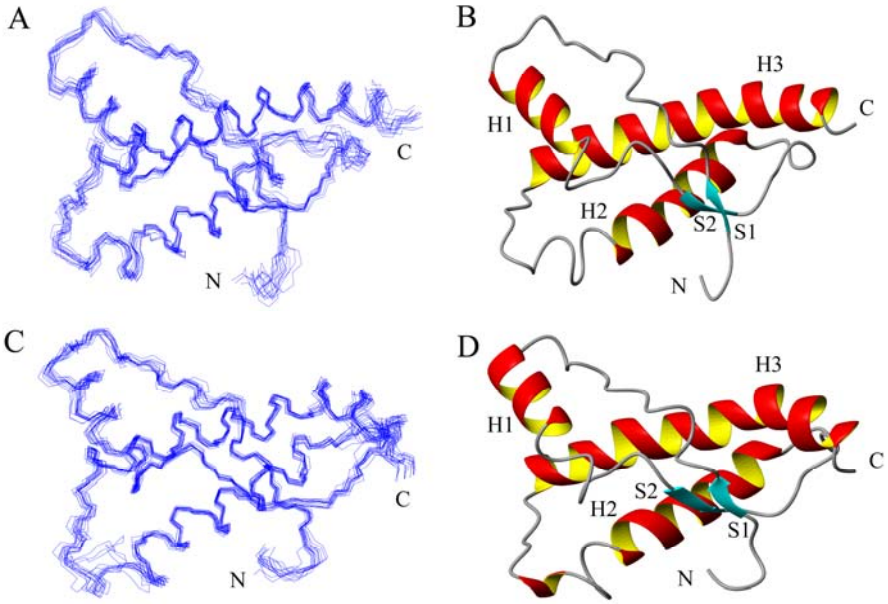

Figure 2

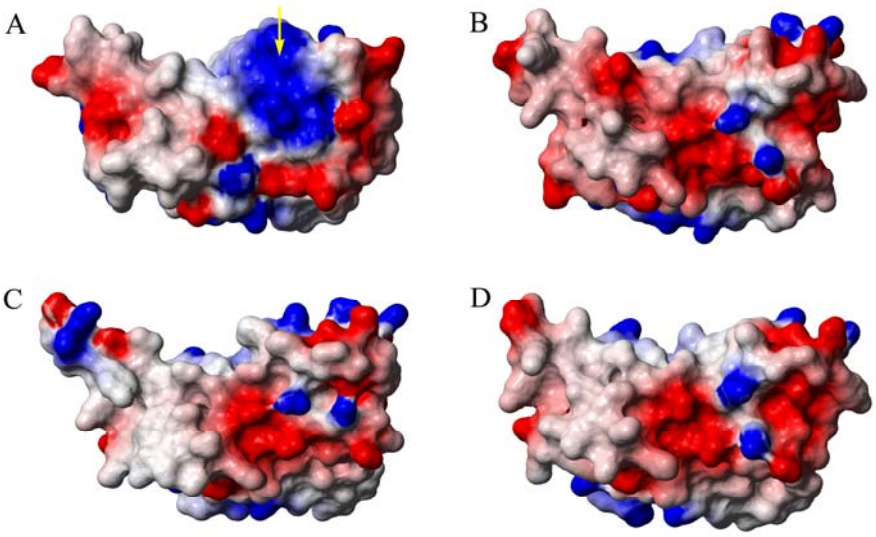

Figure 3

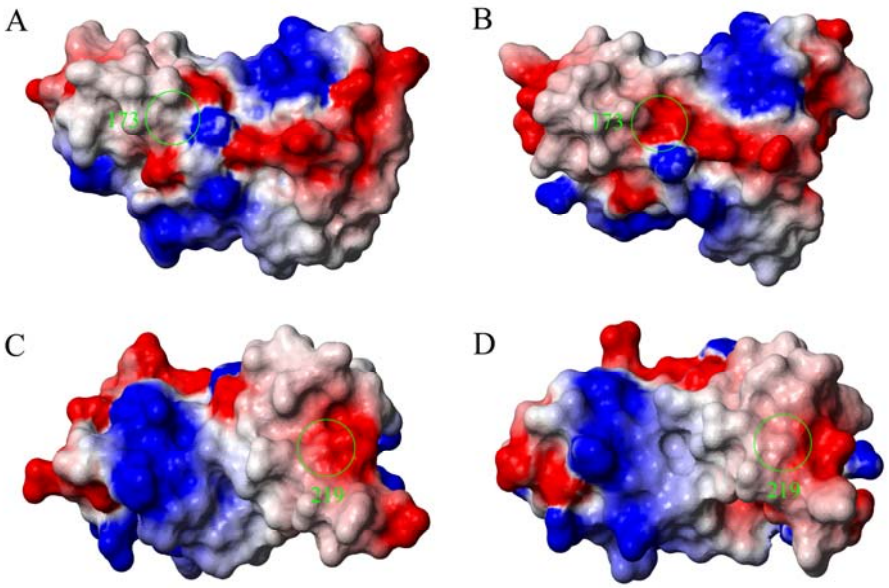

Figure 4

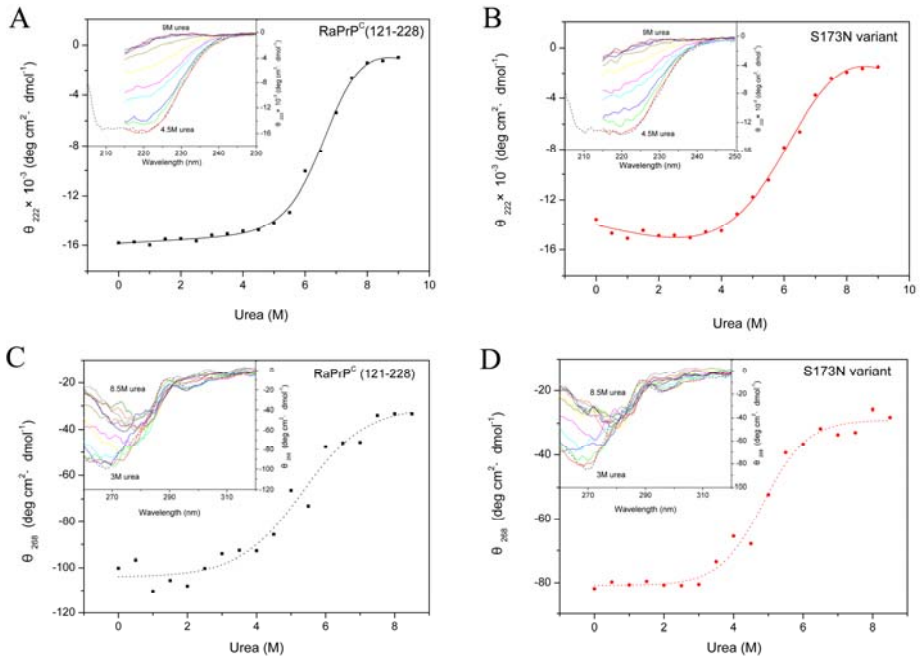

Figure 5

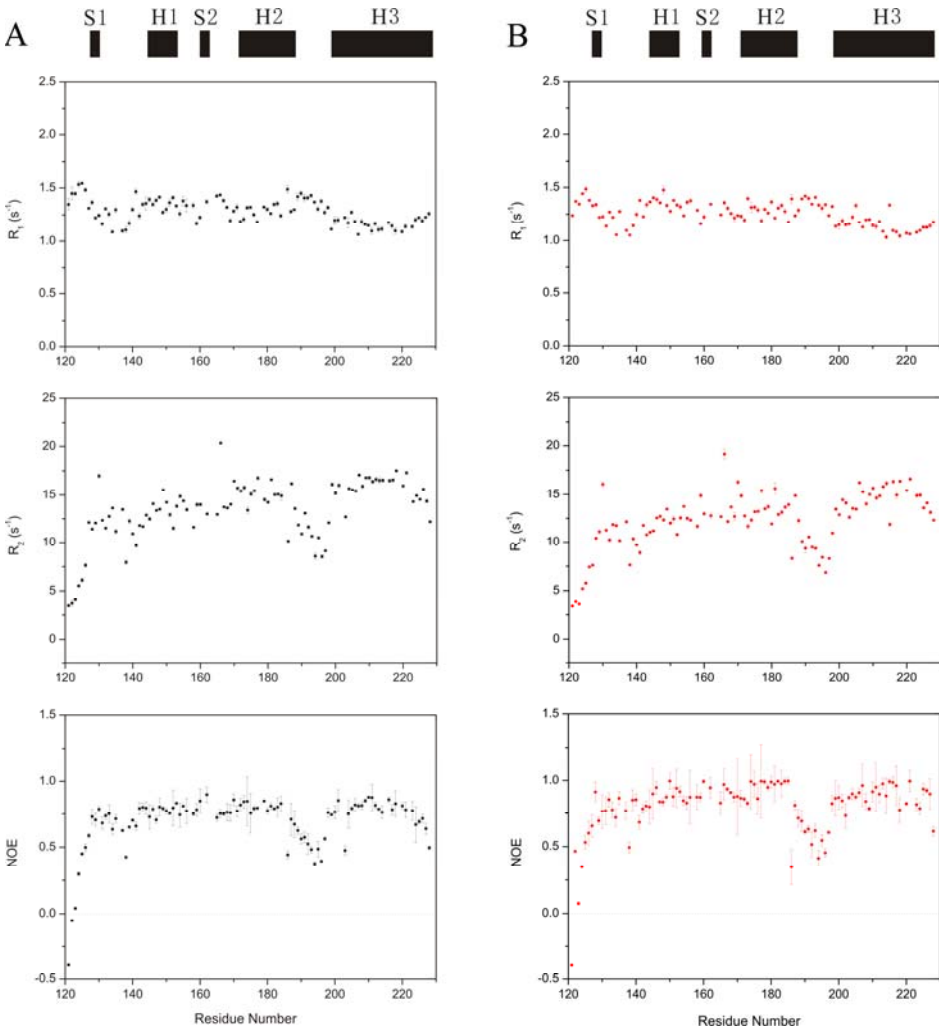

Figure 6

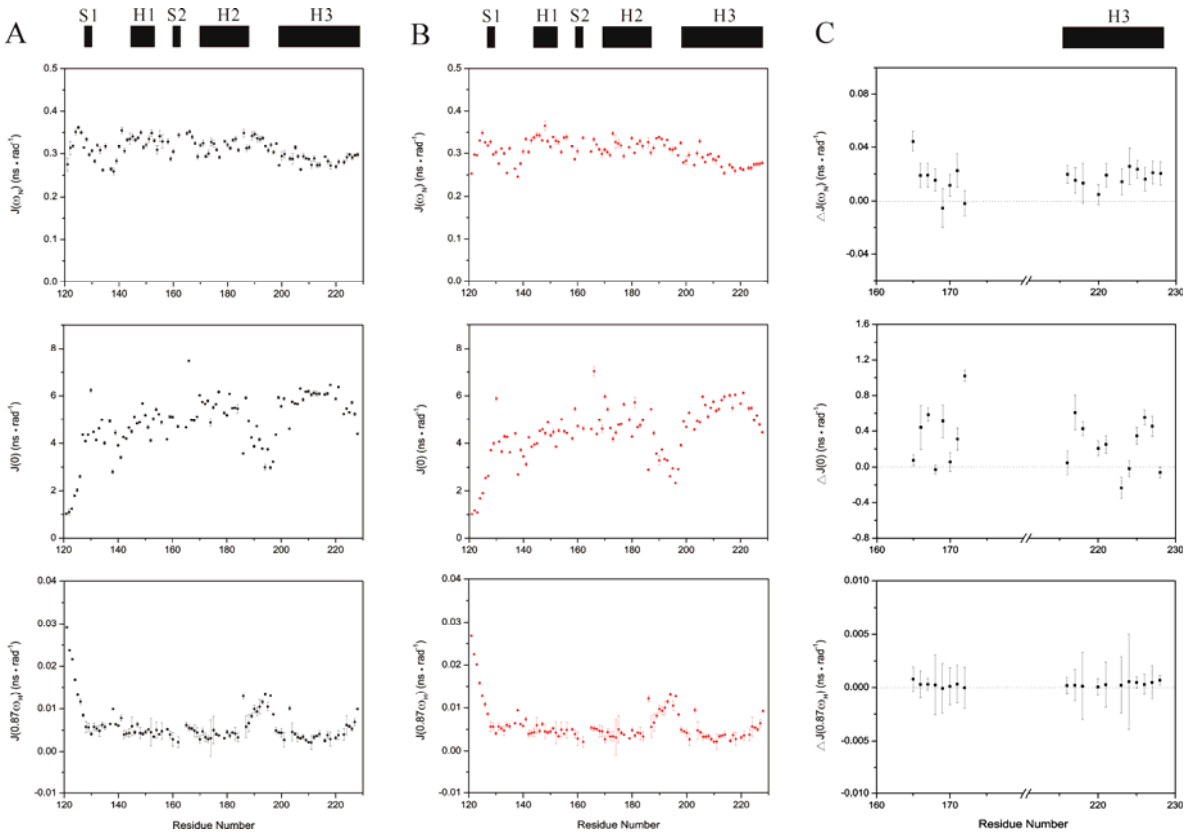

Figure 7